

Tuning the phase diagram of a Rosenzweig-Porter model with fractal disorder

Madhumita Sarkar*

Jožef Stefan Institute, SI-1000, Ljubljana, Slovenia

Roopayan Ghosh

Department of Physics and Astronomy, University College London, Gower Street, WC1E6BT, London

Ivan Khaymovich

Nordita, Stockholm University and KTH Royal Institute of Technology

Hannes Alfvéns väg 12, SE-106 91 Stockholm, Sweden and

Institute for Physics of Microstructures, Russian Academy of Sciences, 603950 Nizhny Novgorod, GSP-105, Russia

Rosenzweig-Porter (RP) model has garnered much attention in the last decade, as it is a simple analytically tractable model showing both ergodic–nonergodic extended and Anderson localization transitions. Thus, it is a good toy model to understand the Hilbert-space structure of many body localization phenomenon. In our study, we present analytical evidence, supported by exact numerical computations, that demonstrates the controllable tuning of the phase diagram in the RP model by employing on-site potentials with a non-trivial fractal dimension instead of the conventional random disorder. We demonstrate that doing so extends the fractal phase and creates unusual dependence of fractal dimensions of the eigenfunctions. Furthermore, we study the fate of level statistics in such a system and analyze the return probability of a wave packet localized at a single site to provide a dynamical test-bed for our theory.

Introduction: Disorder-induced breakdown [1–4] of quantum ergodicity [5, 6], dubbed as many-body localization (MBL), is a generic phenomenon in many-body (MB) systems. Being the localization in real space, MBL is only ergodicity breaking phase in its Hilbert counterpart [7–9]. This fact as well as the discovery of non ergodic extended phases in MB systems [10–21] as an intermediate regime between ergodic and localized phases [1, 22–24] necessitated the search for analytically tractable toy-models to understand the phenomena. One direction of this search led to the random-matrix ensembles that mimic the Hilbert-space properties of such MB systems in a controlled fashion. The Rosenzweig-Porter (RP) random matrix model [25] is such an example which has been studied extensively in recent years as it allows almost a complete analytical understanding of the phase diagram [26–31], and a perturbative (exact in the thermodynamic limit) description [32] of the eigenspectrum for a wide range of parameter values.

The usual RP model is given by the Gaussian random-matrix ensemble of size L , where each element is random number obtained from a normal distribution, and the off-diagonal elements are rescaled by a factor of $L^{-\gamma/2}$,

$$H_{mn} = h_n \delta_{mn} + M_{mn} L^{-\gamma/2}, \quad (1)$$

where $\overline{h_n} = 0$, $\overline{M_{mn}} = 0$, $\overline{h_n^2} = \overline{M_{mn}^2} = 1$. It has been shown that [26, 27], with increasing γ from 0 to large values, this model, first, exhibits ergodicity, and then undergoes a transition to nonergodic extended (fractal) phase at $\gamma = 1$. In the fractal phase the eigenfunctions

are extended over extensive number, but measure zero of all the lattice sites, scaling as L^D , where $D = 2 - \gamma$ denotes the fractal dimension of the eigenfunction. As immediately apparent, $D = 1$ corresponds to the ergodic phase. At $\gamma = 2$, D goes linearly to 0, marking the onset of the Anderson localized phase. While this version of the model lacks genuine multifractality in its eigenfunctions, recent developments [29, 33–37] show that some modified versions of this model may exhibit multifractality. Further studies [38] demonstrated the instability of the nonergodic extended phase in non-Hermitian version of the model.

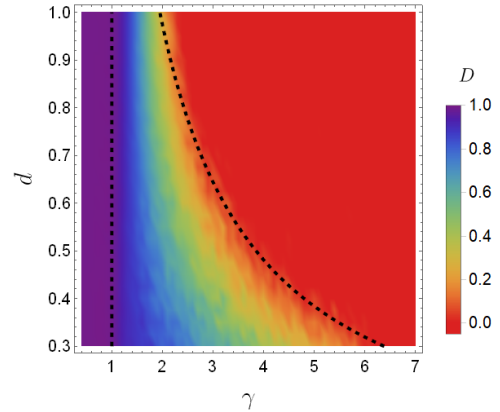


FIG. 1. Fractal dimension D vs γ and the Hausdorff dimension d , showing good agreement with the analytical predictions of ergodic, $\gamma_{ET} \simeq 1$ and Anderson $\gamma_{AT} \simeq 2/d$ transitions (black dotted lines), Eq. (10). Numerically, D_2 has been obtained by fitting the inverse participation ratio (IPR) of the eigenvectors for system sizes $L = 2^p$, $7 \leq p \leq 12$.

* sarkar.madhumita770@gmail.com

Unlike the latter case, in this work we show how to

enhance the range and stability of the fractal phase of the RP model, including a possibility of obtaining nonlinear curves for D versus γ .

Summary of Results: In our study, we selectively employ a random normal distribution solely for the off-diagonal elements of H , while the diagonal elements (H_{mm}) are sourced from a ‘fractal’ disorder distribution with a Hausdorff dimension of d . This implies that there are typically $L^{1-d \times b}$ random diagonal elements, present in an energy window of width L^{-b} , if the total bandwidth is taken to be $O(1)$. One of the well-known examples of such a distribution is the Cantor set with a Hausdorff dimension [39] $d = \ln 2 / \ln 3$.

The main result of our work is shown in Fig. 1, where we represent the extended phase diagram of the RP model in terms of the second fractal dimension D_2 obtained from numerical fits of the generalized IPR, taking $q = 2$.

$$IPR_j^{(q)} = \sum_i^L |\langle i | \chi_j \rangle|^{2q}, \quad (2)$$

where $|i\rangle$ denote computational basis states and $|\chi_j\rangle$ denotes an eigenvector with index j . Then $IPR^{(2)} \sim L^{-D_2}$, one obtains D_2 from averages over numerical fits from a band of eigenvectors. D_2 can then be used to distinguish between ergodic ($= 1$), nonergodic extended, i.e. fractal ($0 < D_2 < 1$) and Anderson localized phase ($= 0$). We shall henceforth refer to D_2 as D since the higher moments show the same value i.e. $D_q = D_2, q > 1/2$, thus indicating that the eigenfunctions are fractal and not multifractal. In Fig. 1, we plot the dependence of D on γ and d . We note the following from the plot,

1. $d = 1$ represents the case for the generic RP model and the ergodic-fractal transition occurs at $\gamma = \gamma_{ET} = 1$ and the Anderson transition occurs at $\gamma = \gamma_{AT} = 2$ replicating the known results [26].
2. As Hausdorff dimension of the diagonal elements decreases, there is no change in γ_{ET} , but γ_{AT} monotonically increases, extending the fractal phase in γ .
3. Both the transitions can be very well approximated by perturbative analytical expressions, which becomes exact in the thermodynamic limit, denoted by black dashed lines in the plot.

It is also worth mentioning that, for $d > 1$, the phase diagram shows similar behaviour as for $d = 1$. This is because beyond the physical dimension of the diagonal disorder (1D in our Hermitian case), any increase in fractal dimension cannot have an effect [40].

In what follows, we, first, analytically compute the fractal dimension for eigenfunctions of the modified RP model with changing γ and d . Then we compare the obtained expressions with exact numerics performed for (i) the commonly studied Cantor set fractal distribution,

and then (ii) for a distribution with arbitrary Hausdorff dimensions d [41]. For completeness, we also discuss the level spacing statistics in such a model, and the time-dependent survival probability of a wave packet initially localized at a single site.

Analytical phase-diagram calculations: As mentioned before, we consider the h_n s to be distributed in a fractal (and later multifractal) manner [42]. This implies that the h_n ’s are distributed such that, the number ($\#$) of h_n ’s in a given energy interval $|E - h_n| \in [L^{-b-db}, L^{-b}]$, parameterized by b ($db \lesssim 1/\ln N$) vary as

$$\# \{ |E - h_n| \in [L^{-b-db}, L^{-b}] \} \equiv L^{1-f(b)} db, \quad (3)$$

with a certain $f(b)$, characterizing the above fractal. We also assume that the overall bandwidth of the h_n is $\sim O(1) = L^0$. Thus, $f(0) = 0$. For any generic fractal with the Hausdorff dimension d we will have,

$$f(b) = d \cdot b, \quad (4)$$

For the special case of the Cantor set, $d = \ln 2 / \ln 3$. In contrast, in the case of uniform disorder distribution, the number of h_n ’s is proportional to the width of the energy interval i.e., $f(b) = b$. Thus the usual Hermitian case [26] corresponds to $d = 1$, while the non-Hermitian complex one [38] gives $d = 2$.

It can also be seen that the typical level spacing of the disorder, δ_{typ} , i.e. the energy interval where one typically finds a single energy level is given by,

$$\begin{aligned} \# &= N^{1-f(b_{typ})} = 1 \quad \Leftrightarrow \quad f(b_{typ}) = 1 \\ &\Leftrightarrow \quad b_{typ} = 1/d \quad \Leftrightarrow \quad \delta_{typ} = L^{-b_{typ}} = L^{-1/d} \end{aligned} \quad (5)$$

In this work, we focus only on real entries and, thus, work in the scenario $0 < d < 1$. Generalization to Non-hermitian matrices to cover $0 \leq d \leq 2$ is straightforward. In what follows, we provide a short description of computation of the fractal dimension of a typical eigenstate of this model and thus compute γ_{AT} and γ_{ET} .

Using the cavity Green’s function method, we can find a self-consistency equation for the level broadening (the imaginary part of the self energy) Γ_m as (see Appendix A and [27, 29, 30]),

$$\bar{\Gamma} = \frac{1}{L} \sum_n \Gamma_n = \sum_n \frac{L^{-\gamma} (\bar{\Gamma} - \delta)}{(E - h_n)^2 + (\bar{\Gamma} - \delta)^2} \quad (6)$$

where E is the eigenenergy of the corresponding eigenvector. Since δ is a small regularization offset, in the limit $\delta \rightarrow 0$, and parameterizing $\bar{\Gamma} = L^{-a}$, within the saddle-point approximation Eq. (6) gives the following result, (see Appendix A for more details)

$$1 \sim L^{1-\gamma+2a-f(a)} \quad \Leftrightarrow \quad \gamma = 1 + 2a - f(a), \quad (7)$$

This determines $\Gamma \sim L^{-a}$ via the parameter γ .

Now, we can determine the fractal dimension $D_q \equiv D$, via the number of levels located in the interval $\Gamma \sim L^{-a}$,

which is related to the fractal dimension as L^D . From Eq. (3), we know that this is given by $L^{1-f(a)}$. Thus,

$$D = 1 - f(a). \quad (8)$$

This definition of D is the fractality in the “space” of h_n , but for the RP-like fractal phases it is equal to the spatial fractal dimension due to the Lorentzian structure of the eigenstates [29, 30, 38, 43, 44]:

$$\langle |\psi_E(n)|^2 \rangle_{H_{m \neq n}} \sim \frac{1}{(E - h_n)^2 + \Gamma^2}. \quad (9)$$

As by fixing either E or h_n , one has the Lorentzian, the fractality over the energy E and over the “space” h_n is equivalent to each other. In space n , the above Lorentzian forms a fractal miniband [39] of the width Γ , with the underlying fractal structure h_n , living in that miniband, $|h_n - E| \lesssim \Gamma$.

For the fractal case, Eq. (4), using Eqs. (7) - (8), we obtain for $\gamma > 1$,

$$D = \max \left(1 - d \frac{\gamma - 1}{2 - d}, 0 \right), \quad \Gamma \sim L^{-\frac{\gamma-1}{2-d}}. \quad (10)$$

To find the Anderson transition point we realize that there $\Gamma \simeq \delta_{typ}$, i.e., $D = 0$, since in the localized phase the number of energy levels in the bandwidth becomes an intensive quantity. Hence, $a = b_{typ} = 1/d$, i.e.

$$\gamma_{AT} = 2/d, \quad (11)$$

The ergodic transition occurs at $\Gamma \sim O(1)$, $\gamma_{ET} = 1$. Note that both γ_{ET} and γ_{AT} are continuous transitions, unlike the fat-tailed distributed RP models [33–35].

Cantor Set diagonal elements: The first example we consider is when the diagonal elements are represented by Cantor set, \mathcal{C} . Cantor set is a set of points lying in a line segment normalized to the interval $[0, 1]$, obtained by removing the middle third of the continuous line segments in a recursive manner. The set generated by the first few iterations of this are,

$$\begin{aligned} \mathcal{C}_0 &= [0, 1] \\ \mathcal{C}_1 &= \left[0, \frac{1}{3}\right] \cup \left[\frac{2}{3}, 1\right] \\ \mathcal{C}_2 &= \left[0, \frac{1}{9}\right] \cup \left[\frac{2}{9}, \frac{1}{3}\right] \cup \left[\frac{2}{3}, \frac{7}{9}\right] \cup \left[\frac{8}{9}, 1\right] \\ &\dots \end{aligned} \quad (12)$$

We generate the diagonal elements by choosing the boundary value of each subset at the $n = \log_2 L$ iteration. The self similar nature of the Cantor set is evident from the construction and the Hausdorff dimension is calculated to be $d = \frac{\ln 2}{\ln 3}$. [45].

In Fig. 2 (a) we plot the second fractal dimension $D_2 = D$ calculated from numerical fitting in system size $2^p, p = 7 \dots 12$, for all the eigenvectors arranged in increasing order of IPR. In Fig. 2 (b) we plot the same

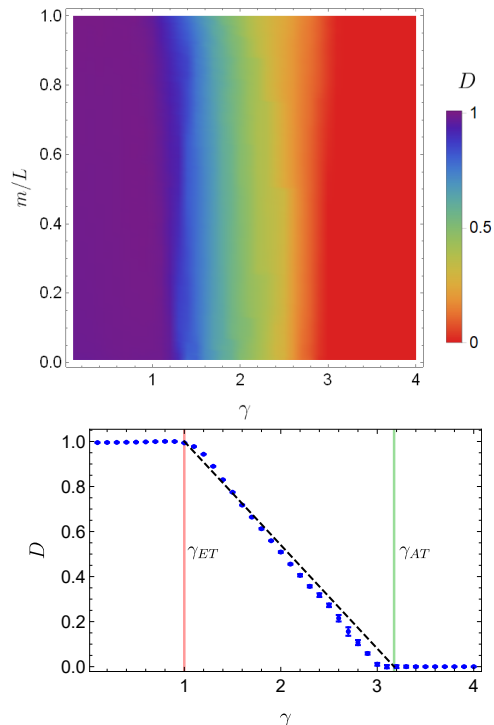


FIG. 2. Variation of fractal dimension D of the eigenspectrum with γ for Cantor set disorder. (a) Plot of fractal dimension D as a function of eigenvector index m/L (after sorting in increasing order of IPR) and γ . Right: Plot of fractal dimension (denoted by blue dots) D as a function of γ averaged over all eigenstates. Black dashed line indicates the fractal dimension calculated in Eq. (10) for $1 < \gamma < \gamma_{AT}$, with $d = \frac{\ln 2}{\ln 3} \sim 0.63$. Red vertical line indicate the theoretical predictions of the $\gamma_{ET} = 1$ and green vertical line indicate the theoretical prediction of γ_{AT} in Eq. (11).

quantity but averaged over 60 mid spectrum states. From Fig. 2 (a) it can be clearly seen that there is no mobility edge in the spectrum, all the eigenstates show similar fractal dimensions D , hence one can average over them, which is plotted in Fig. 2 (b). The point where the system ceases to be ergodic is clearly visible at $\gamma = \gamma_{ET} = 1$. Furthermore the variation of the fractal dimension of the eigenfunctions D matches sufficiently well with the analytically obtained black dashed line, Eq. (10), in the $\gamma_{ET} < \gamma < \gamma_{AT}$ regime, thus accurately predicting the γ_{AT} point as well.

Generic d diagonal elements: Next, we consider the case of completely generic fractal diagonal elements. The generation of diagonal elements distributed in a generic fractal dimension was introduced recently in Ref. 39, this section also serves as a demonstration of applicability of the technique. Below, we give a short summary of the method.

A random fractal spectrum of Hausdorff dimension d can be generated using i.i.d. non-negative level spacings

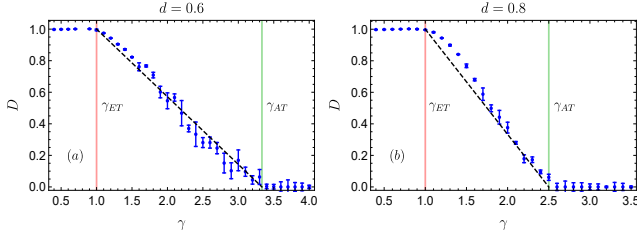


FIG. 3. Plot of fractal dimension D as a function of γ averaged over all eigenstates for generic fractal diagonal disorder with Hausdorff dimension d for (a) $d = 0.6$ and (b) $d = 0.8$. The lines and rest of the parameters are same as Fig. 2.

of ordered $h_n \leq h_{n+1}$

$$s_n \equiv h_{n+1} - h_n \Leftrightarrow h_n = h_0 + \sum_{k=0}^{n-1} s_k \quad (13)$$

which is distributed as a Pareto distribution [46]

$$P(s) = \frac{d\delta_{typ}^d}{s^{d+1}} \theta(s - \delta_{typ}) , \quad (14)$$

where $\delta_{typ} \sim N^{-1/d}$, is the typical level spacing of the model and we omit the subscript n for brevity. Indeed, one can count that for the usual Cantor set with $d = \ln 2 / \ln 3$, at n^{th} step one keeps $N \cdot P(s) \sim 2^n$ levels with the spacings $s \sim 3^{-n}$, leading to the above expression. Due to the formal divergence of the mean level spacing for all $d < 1$ at large s , for any finite L one should put an

upper cutoff $s_{\max} O(1)$, given by the entire bandwidth:

$$\delta = \langle s \rangle \sim \int_{\delta_{typ}}^{s_{\max}} s P(s) ds \sim \delta_{typ}^d \sim L^{-1} \quad (15)$$

and consider a typical realization where there is the only $s_n \simeq s_{\max} \simeq O(1)$, determining the bandwidth.

In Fig. 3 (a) and (b) we demonstrate how our theoretical predictions of D match with numerical results for $d = 0.6$ and $d = 0.8$. We see that even for generic dimensions our analytical predictions match very well with numerics.

Multifractal disorder: As a final example, we consider the more general case of multifractal disorder. Unlike the fractal case, where the scaling behaviour of all the moments of the distribution are the same, in a multifractal they are a nontrivial function of the moment order. Thus, one needs to define the probability distribution of level spacings in an energy window appropriately scaling with system size. Relegating the details to the Appendix B, we directly provide the probability distribution of level spacings below,

$$P(s \sim N^{-\nu}) ds = \sqrt{\frac{|g''(\nu_0)| \ln N}{2\pi}} N^{g(\nu)-1} d\nu \quad (16)$$

where $g(\nu)$ is a non-linear function of ν . As an example we consider the particular case of the log-normal distribution where, $g(\nu) = 1 - \frac{(\nu - \nu_0)^2}{4(\nu_0 - 1)}$.

Then we can compute the fractal dimension D (see Appendix B) as,

$$D(\gamma) = \begin{cases} 1, & \gamma < 1 \\ 2 - \gamma, & 1 < \gamma < 3 - \nu_0 \\ \frac{\gamma + 6\nu_0 - 8 - 4\sqrt{(\nu_0 - 1)(\gamma + 2\nu_0 - 4)}}{0}, & 3 - \nu_0 < \gamma < 2\nu_0 \\ 0, & \gamma > 2\nu_0 \end{cases} \quad (17)$$

where the Anderson transition happens at $D = 0$, i.e., at $b = \nu_0$ and $\gamma = 2\nu_0$. The above formula works for $1 < \nu_0 < 2$. Note that unlike the fractal case, here there are 4 regimes: (i) ergodic phase, $\Gamma \gg O(1)$; (ii) usual fractal case, $\delta \ll \Gamma \ll O(1)$; (iii) new fractal case, $\delta_{typ} \ll \Gamma \ll \delta$; (iv) localized phase, $\Gamma \ll \delta_{typ}$. Here the unusual fractal phase (iii) appears only when the mean level spacing δ converges and differs from the typical one, $\delta_{typ} \ll \delta \ll O(1)$.

The results are plotted in Fig. 4 where the predicted fractal dimensions from our saddle point approximation match well with exact numerical results. We clearly see a curvature in D vs γ , a feature absent in the fractal case, which increases with increasing ν_0 . However it seems that corrections to the saddle point approximation are stronger in this case than for fractal disorder, due to the logarithmic dependence of the prefactors in Eq. (16).

To complete the analysis, now we discuss how the features of the phase transition are ingrained in the eigenvalues using level statistics and in the dynamics via computation of survival probability.

a. Level statistics: Here, we focus on the consecutive level spacing ratio, r defined by,

$$r = \frac{\min(\delta_n, \delta_{n+1})}{\max(\delta_n, \delta_{n+1})} \quad (18)$$

where $\delta_n = E_n - E_{n+1}$, E_n is the n^{th} eigenvalue sorted in increasing order. In the ergodic phase, it is well known that using the Gaussian Orthogonal Ensemble (GOE) ansatz, [47, 48] $p(r) = \frac{27}{4} \frac{r+r^2}{(1+r+r^2)^{5/2}}$ giving $\langle r \rangle \sim 0.535$. Deep in the localized phase we compute

$$p(r) = \frac{d}{r^{1-d}}, \text{ which gives } \langle r \rangle = \frac{d}{d+1}. \quad (19)$$

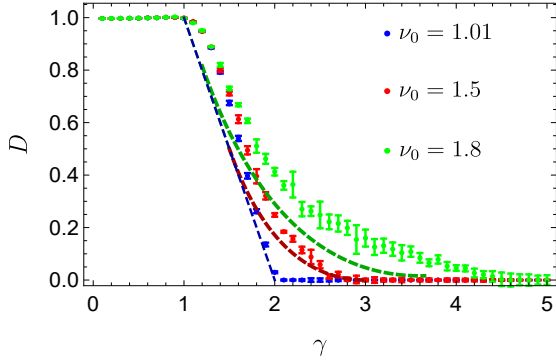


FIG. 4. The plot of $D(\gamma)$ as a function of γ for $\nu_0 = 1.01$ (blue), $\nu_0 = 1.5$ (red), $\nu_0 = 1.8$ (green). The dotted lines are the analytical estimates of $D(\gamma)$ from Eq. (17).

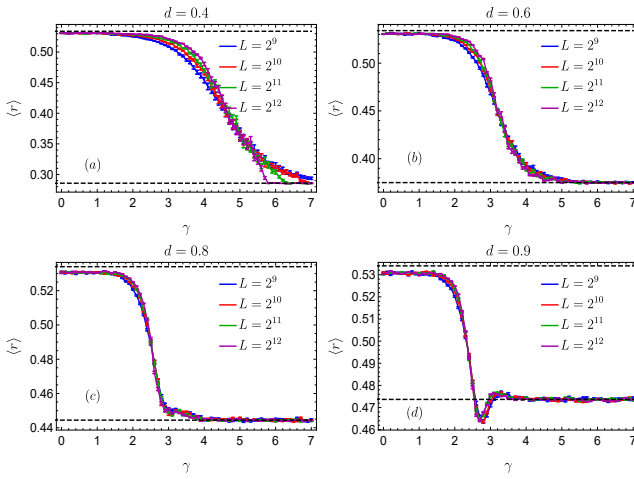


FIG. 5. Plot of $\langle r \rangle$ as a function of γ for (a) $d = 0.4$, (b) $d = 0.6$, (c) $d = 0.8$, Bottom Left: (d) $d = 0.9$, for different system sizes L . The black dashed lines denote the expected values of $\langle r \rangle$ for GOE statistics and localized phase.

In Fig. 5 we plot the variation of $\langle r \rangle$ with γ for different d . As expected from our analysis for $\gamma < \gamma_{ET} = 1$, it admits value close to 0.535, while at large $\gamma > \gamma_{AT} = 2/d$, it settles at $\sim \frac{d}{d+1}$, Eq. (19). As the smaller d -values corresponds to the fatter distribution tail Eq. (14), the finite size effects are stronger.

According to Eq. (9), γ -dependence of $\langle r \rangle$ goes to a kink at $\gamma = \gamma_{AT}$ in the thermodynamic limit. An interesting aspect is another ‘kink’, observed in the plots for $d \gtrsim 0.9$. While the first kink is due to breakdown of level repulsion, the second kink occurs due to the fat tail of $P(r)$ in the localized phase for $d \sim 1$. When the weight of large r values for non-hybridized eigenstates deep inside the localized phase become significantly larger than what it was in the ergodic or fractal phase, it shows up as a slight increase in $\langle r \rangle$. See Appendix C for more details.

b. Survival probability: In this section we consider the time dependence of the survival (or return)

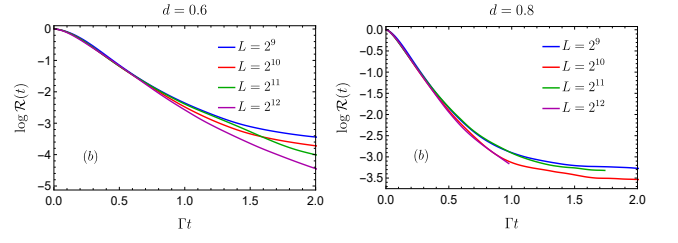


FIG. 6. Plot of survival probability in the NEE region for $\gamma = 2$ at (a) $d = 0.6$ and (b) $d = 0.8$.

probability, $R(t)$ [43], defined by,

$$R(t) = |\langle \psi(0) | e^{-iHt} | \psi(0) \rangle|^2, \quad (20)$$

in various regimes. We consider the initial wave function is localized on a single site, N , i.e. $|\psi(0)\rangle = \sum_{i=1}^L \delta_{iN} \langle i | \psi(0) \rangle$.

Like in the standard RP-model [43], in the NEE phase $\mathcal{R}(t) \sim e^{-\Gamma t}$, where $\Gamma = L^{-\frac{2-d}{2-d}}$, Eq. (10). In Fig. 6 we see that after rescaling the time by Γ , the curves for different L s overlap with one another for different d . The exponential behavior of the return probability is given by the Lorentzian wave-function profile Eq. (9) in the energy domain. Similarly to the standard RP case [43], one can calculate the return probability from its Fourier transform $K(\omega)$, which for the Lorentzian profile is also Lorentzian.

Discussion: In this work, we have demonstrated that making the distribution of the diagonal elements to be fractal in the RP model allows one to adjust the phase diagram and change the location of the Anderson localization transition γ_{AT} . We have derived an analytical expression Eq. (10) that relates the Hausdorff dimension of the disorder to the fractal dimension of the eigenstates in the RP Hamiltonian, and have confirmed our findings through exact numerical computations. Furthermore, we have shown that we can manipulate the disorder dependence of the fractal dimension by utilizing a multifractal disorder. Finally, we have evaluated the implications of our modification on the eigenspectrum through level spacing ratio, and on the dynamics through survival probability.

This work gives the first step in the direction of usage of the fractal disorder for the controllable tunability of the phase diagrams of various disordered models.

In particular, this work opens the way to study, whether such fractal diagonal disorder enhances fractality of wave functions in other long-range models, such as the power law banded models [49], Burin-Maksimov model [50–53], some Bethe-ansatz integrable ones [54–56], on the random graphs [57, 58], or even in the interacting disordered models [4]. In all these cases (especially in the latter two), the fractal disorder may open a room for non-ergodic spatially extended phase of matter, intensively discussed and highly relevant for quantum algorithms [59] and machine learning [60]. The analysis of

spectral statistics for $d \sim 1$ using spectral form factor can also show interesting behaviour at different timescales near γ_{AT} , which can help to identify more clearly the origin of the sudden dip in the $\langle r \rangle$ statistics and shed light on spectral distribution in the critical (fractal) regime of ergodic-localized phase transitions and structure of fractal minibands [39].

I. ACKNOWLEDGMENTS

I. M. K. acknowledges the support by the European Research Council under the European Union's Seventh Framework Program Synergy ERC-2018-SyG HERO-810451. M.S. acknowledges support of the projects J1-2463 of the Slovenian Research Agency and EU via QuantERA grant T-NiSQ. R.G. acknowledges support from UKRI Grant No. EP/R029075/1.

-
- [1] F. Evers and A. D. Mirlin, Anderson transitions, *Rev. Mod. Phys.* **80**, 1355 (2008).
 - [2] D. Basko, I. Aleiner, and B. Altshuler, Metal-insulator transition in a weakly interacting many-electron system with localized single-particle states, *Annals of Physics* **321**, 1126 (2006).
 - [3] I. V. Gornyi, A. D. Mirlin, and D. G. Polyakov, Interacting electrons in disordered wires: Anderson localization and low- t transport, *Phys. Rev. Lett.* **95**, 206603 (2005).
 - [4] D. A. Abanin, E. Altman, I. Bloch, and M. Serbyn, Colloquium: Many-body localization, thermalization, and entanglement, *Rev. Mod. Phys.* **91**, 021001 (2019).
 - [5] J. M. Deutsch, Quantum statistical mechanics in a closed system, *Phys. Rev. A* **43**, 2046 (1991).
 - [6] M. Srednicki, Chaos and quantum thermalization, *Phys. Rev. E* **50**, 888 (1994).
 - [7] D. J. Luitz, N. Laflorencie, and F. Alet, Many-body localization edge in the random-field Heisenberg chain, *Phys. Rev. B* **91**, 081103 (2015).
 - [8] N. Macé, F. Alet, and N. Laflorencie, Multifractal scalings across the many-body localization transition, *Phys. Rev. Lett.* **123**, 180601 (2019).
 - [9] G. De Tomasi, I. M. Khaymovich, F. Pollmann, and S. Warzel, Rare thermal bubbles at the many-body localization transition from the Fock space point of view, *Phys. Rev. B* **104**, 024202 (2021).
 - [10] Y. Bar Lev, G. Cohen, and D. R. Reichman, Absence of diffusion in an interacting system of spinless fermions on a one-dimensional disordered lattice, *Phys. Rev. Lett.* **114**, 100601 (2015).
 - [11] K. Agarwal, S. Gopalakrishnan, M. Knap, M. Müller, and E. Demler, Anomalous diffusion and Griffiths effects near the many-body localization transition, *Phys. Rev. Lett.* **114**, 160401 (2015).
 - [12] D. J. Luitz, N. Laflorencie, and F. Alet, Extended slow dynamical regime close to the many-body localization transition, *Phys. Rev. B* **93**, 060201 (2016).
 - [13] D. J. Luitz and Y. Bar Lev, Anomalous thermalization in ergodic systems, *Phys. Rev. Lett.* **117**, 170404 (2016).
 - [14] I. Khait, S. Gazit, N. Y. Yao, and A. Auerbach, Spin transport of weakly disordered Heisenberg chain at infinite temperature, *Phys. Rev. B* **93**, 224205 (2016).
 - [15] M. Žnidarič, A. Scardicchio, and V. K. Varma, Diffusive and subdiffusive spin transport in the ergodic phase of a many-body localizable system, *Phys. Rev. Lett.* **117**, 040601 (2016).
 - [16] Y. Bar Lev, D. M. Kennes, C. Klöckner, D. R. Reichman, and C. Karrasch, Transport in quasiperiodic interacting systems: From superdiffusion to subdiffusion, *EPL (Europhysics Letters)* **119**, 37003 (2017).
 - [17] S. Bera, G. De Tomasi, F. Weiner, and F. Evers, Density propagator for many-body localization: Finite-size effects, transient subdiffusion, and exponential decay, *Phys. Rev. Lett.* **118**, 196801 (2017).
 - [18] K. Agarwal, E. Altman, E. Demler, S. Gopalakrishnan, D. A. Huse, and M. Knap, Rare-region effects and dynamics near the many-body localization transition, *Annalen der Physik* **529**, 1600326 (2017).
 - [19] D. J. Luitz and Y. Bar Lev, The ergodic side of the many-body localization transition, *Annalen der Physik* **529**, 1600350 (2017).
 - [20] T. L. M. Lezama, S. Bera, and J. H. Bardarson, Apparent slow dynamics in the ergodic phase of a driven many-body localized system without extensive conserved quantities, *Phys. Rev. B* **99**, 161106 (2019).
 - [21] S. Roy, Y. Bar Lev, and D. J. Luitz, Anomalous thermalization and transport in disordered interacting Floquet systems, *Physical Review B* **98**, 060201 (2018).
 - [22] S. Roy, I. M. Khaymovich, A. Das, and R. Moessner, Multifractality without fine-tuning in a Floquet quasiperiodic chain, *SciPost Phys.* **4**, 25 (2018).
 - [23] M. Sarkar, R. Ghosh, A. Sen, and K. Sengupta, Mobility edge and multifractality in a periodically driven Aubry-André model, *Phys. Rev. B* **103**, 184309 (2021).
 - [24] M. Sarkar, R. Ghosh, A. Sen, and K. Sengupta, Signatures of multifractality in a periodically driven interacting Aubry-André model, *Phys. Rev. B* **105**, 024301 (2022).
 - [25] N. Rosenzweig and C. E. Porter, "repulsion of energy levels" in complex atomic spectra, *Phys. Rev. B* **120**, 1698 (1960).
 - [26] V. E. Kravtsov, I. M. Khaymovich, E. Cuevas, and M. Amini, A random matrix model with localization and ergodic transitions, *New J. Phys.* **17**, 122002 (2015).
 - [27] D. Facchetti, P. Vivo, and G. Biroli, From non-ergodic eigenvectors to local resolvent statistics and back: A random matrix perspective, *Europhys. Lett.* **115**, 47003 (2016).
 - [28] K. Truong and A. Ossipov, Eigenvectors under a generic perturbation: Non-perturbative results from the random matrix approach, *Europhys. Lett.* **116**, 37002 (2016).
 - [29] C. Monthus, Statistical properties of the Green function in finite size for Anderson localization models with multifractal eigenvectors, *J. Phys. A: Math. Theor.* **50**, 295101 (2017).
 - [30] E. Bogomolny and M. Sieber, Eigenfunction distribution for the Rosenzweig-Porter model, *Phys. Rev. E* **98**, 032139 (2018).

- [31] D. Venturelli, L. F. Cugliandolo, G. Schehr, and M. Tarzia, Replica approach to the generalized Rosenzweig-Porter model, *SciPost Phys.* **14**, 110 (2023).
- [32] P. von Soosten and S. Warzel, Non-ergodic delocalization in the Rosenzweig-Porter model, *Letters in Mathematical Physics*, **1** (2018).
- [33] V. E. Kravtsov, I. M. Khaymovich, B. L. Altshuler, and L. B. Ioffe, Localization transition on the random regular graph as an unstable tricritical point in a log-normal Rosenzweig-Porter random matrix ensemble, *arXiv:2002.02979* (2020).
- [34] I. M. Khaymovich, V. E. Kravtsov, B. L. Altshuler, and L. B. Ioffe, Fragile ergodic phases in logarithmically-normal Rosenzweig-Porter model, *Phys. Rev. Research* **2**, 043346 (2020).
- [35] G. Biroli and M. Tarzia, Lévy-Rosenzweig-Porter random matrix ensemble, *Phys. Rev. B* **103**, 104205 (2021).
- [36] I. M. Khaymovich and V. E. Kravtsov, Dynamical phases in a “multifractal” Rosenzweig-Porter model, *SciPost Phys.* **11**, 45 (2021).
- [37] A. G. Kutlin and I. M. Khaymovich, *Anatomy of the eigenstates distribution: a quest for a genuine multifractality* (2023), in preparation.
- [38] G. De Tomasi and I. M. Khaymovich, Non-hermitian rosenzweig-porter random-matrix ensemble: Obstruction to the fractal phase, *Phys. Rev. B* **106**, 094204 (2022).
- [39] B. Altshuler and V. Kravtsov, Random cantor sets and mini-bands in local spectrum of quantum systems (2023).
- [40] Unlike the non-Hermitian case, where $1 < d < 2$ does change the phase diagram [38].
- [41] The distribution is generated using the method discussed in Ref. 39.
- [42] Note that the strength of the diagonal elements is obtained from a fractal distribution, and not their spatial spread.
- [43] G. de Tomasi, M. Amini, S. Bera, I. M. Khaymovich, and V. E. Kravtsov, Survival probability in generalized Rosenzweig-Porter random matrix ensemble, *SciPost Phys.* **6**, 014 (2019).
- [44] W. Buijsman and Y. B. Lev, Circular Rosenzweig-Porter random matrix ensemble, *SciPost Phys.* **12**, 82 (2022).
- [45] O. Dovgoshey, O. Martio, V. Ryazanov, and M. Vuorinen, The cantor function, *Expositiones Mathematicae* **24**, 1 (2006).
- [46] B. C. Arnold, *Pareto distributions* (International cooperative Publishing House, 1983).
- [47] V. Oganessian and D. A. Huse, Localization of interacting fermions at high temperature, *Phys. Rev. B* **75**, 155111 (2007).
- [48] Y. Y. Atas, E. Bogomolny, O. Giraud, and G. Roux, Distribution of the ratio of consecutive level spacings in random matrix ensembles, *Phys. Rev. Lett.* **110**, 084101 (2013).
- [49] A. D. Mirlin, Y. V. Fyodorov, F.-M. Dittes, J. Quezada, and T. H. Seligman, Transition from localized to extended eigenstates in the ensemble of power-law random banded matrices, *Phys. Rev. E* **54**, 3221 (1996).
- [50] A. L. Burin and L. A. Maksimov, Localization and delocalization of particles in disordered lattice with tunneling amplitude with r^{-3} decay, *JETP Lett.* **50**, 338 (1989).
- [51] X. Deng, V. Kravtsov, G. Shlyapnikov, and L. Santos, Duality in power-law localization in disordered one-dimensional systems, *Phys. Rev. Lett.* **120**, 110602 (2018).
- [52] P. A. Nosov, I. M. Khaymovich, and V. E. Kravtsov, Correlation-induced localization, *Physical Review B* **99**, 104203 (2019).
- [53] X. Deng, A. L. Burin, and I. M. Khaymovich, Anisotropy-mediated reentrant localization, *SciPost Phys.* **13**, 116 (2022).
- [54] R. Richardson, A restricted class of exact eigenstates of the pairing-force Hamiltonian, *Phys. Lett.* **3**, 277 (1963).
- [55] R. Richardson and N. Sherman, Exact eigenstates of the pairing-force Hamiltonian, *Nuclear Physics* **52**, 221 (1964).
- [56] R. Modak, S. Mukerjee, E. A. Yuzbashyan, and B. S. Shastri, Integrals of motion for one-dimensional Anderson localized systems, *New J. Phys.* **18**, 033010 (2016).
- [57] V.E.Kravtsov, B.L.Altshuler, and L.B.Ioffe, Non-ergodic delocalized phase in Anderson model on Bethe lattice and regular graph, *Annals of Physics* **389**, 148 (2018).
- [58] K. Tikhonov and A. Mirlin, From Anderson localization on random regular graphs to many-body localization, *Annals of Physics*, 168525 (2021).
- [59] V. N. Smelyanskiy, K. Kechedzhi, S. Boixo, S. V. Isakov, H. Neven, and B. Altshuler, Nonergodic delocalized states for efficient population transfer within a narrow band of the energy landscape, *Phys. Rev. X* **10**, 011017 (2020).
- [60] K. Kechedzhi, V. N. Smelyanskiy, J. R. McClean, V. S. Denchev, M. Mohseni, S. V. Isakov, S. Boixo, B. L. Altshuler, and H. Neven, Efficient population transfer via non-ergodic extended states in quantum spin glass, *arXiv:1807.04792* (2018).

Appendix A: Derivation of Eq. (6) and Eq. (7)

The cavity Green’s function method is a technique to self consistently solve the Green’s function of a system by connecting the complete Green’s function of the system to the Green’s function with a single site removed. Green’s function is defined as

$$G(E + i\delta) = (E + i\delta - H)^{-1}. \quad (\text{A1})$$

Using the Schur’s complement formula at the removed site m , the cavity equation takes the form [27, 29, 30]

$$G_{mm}(E+i\delta) = \left(E + i\delta - h_m + \sum_{n,r \neq m} H_{mn} G_{nr}^{(m)} H_{rm} \right)^{-1} \quad (\text{A2})$$

where $G^{(m)}$ denotes the Green’s function with the m^{th} row and column removed, $H_{mn} = L^{-\gamma/2} M_{mn}$.

As the self-energy $\Sigma = \sum_{n,r \neq m} H_{mn} G_{nr}^{(m)} H_{rm}$ is self-averaging for not fat-tail distributed $H_{m \neq n}$, following the literature [27, 30, 38], one can consider only diagonal part of it, which is not averaged out

$$\Sigma \simeq \bar{\Sigma} = \sum_n \overline{H_{mn}^2 G_{nn}^{(m)}} = L^{-\gamma} \sum_n G_{nn}. \quad (\text{A3})$$

In the last equality we have replaced $G^{(m)}$ by G , which is exact in the thermodynamic limit, and substituted the variance of $H_{m \neq n}$.

Substituting Eq. (A2) into the latter, one obtains the self-consistency equation

$$\bar{\Sigma} = \sum_n \frac{L^{-\gamma}}{E - h_n + i\delta + \bar{\Sigma}} \quad (\text{A4})$$

which is equivalent to Eq. (6) for $\bar{\Gamma} = \text{Im } \bar{\Sigma}$ and neglected $\text{Re } \bar{\Sigma} \ll E, \epsilon_i$.

Then without loss of generality, we can rewrite Eq. (6) as,

$$\begin{aligned} 1 &= \sum_n \frac{L^{-\gamma}}{|E - h_n|^2 + \bar{\Gamma}^2} \\ &= \sum_b L^{1-f(b)} \frac{L^{-\gamma}}{L^{-2b} + L^{-2a}} \\ &\simeq \sum_{b < a} L^{1-\gamma-f(b)+2b} + \sum_{b > a} L^{1-\gamma-f(b)+2a} \end{aligned} \quad (\text{A5})$$

In the second step we have changed the summation index from n to b , using the fact that the number of levels with $|E - h_n| \sim L^{-b}$ is $L^{1-f(b)}$, and in the third step we approximated the denominator by the larger of L^{-2b} and L^{-2a} at the appropriate values of b , since that is the dominant term as $L \rightarrow \infty$.

To evaluate the expression, notice that the function in the first part is monotonically increasing with b , while in the second one it is monotonically decreasing with b . Then, within the saddle-point approximation (ignoring the pre-factors), the sum is given by the maximal value of the summand at $b = a$. Doing so we arrive at Eq. (7) in the main text.

Appendix B: Multifractal disorder

In order to realize a multifractal disorder, following the same idea as in Eqs. (13), (14), one should take a generic multifractal probability distribution $P(s)$ (written in a saddle-point approximation)

$$\begin{aligned} P(s \sim N^{-\nu}) ds &\sim N^{g(\nu)-1} d\nu, \\ \max_{\nu} g(\nu) &\equiv g(\nu_0) = 1, \\ \max_{\nu} [g(\nu) - q\nu] &\equiv g(\nu_q) - q \cdot \nu_q, \end{aligned} \quad (\text{B1})$$

where we introduced the notations ν_q for the moments

$$\langle s^q \rangle \sim N^{g(\nu_q)-1-q\nu_q}, \quad (\text{B2})$$

to which the main contribution is given by $s_q \sim N^{-\nu_q}$. $\delta_{typ} \sim N^{-\nu_0}$ is the typical (most probable) value of s , while the mean-level spacing, given by the first moment (if it converges)

$$\delta = \langle s \rangle \sim N^{g(\nu_1)-\nu_1-1} \sim 1/N \quad \Leftrightarrow \quad g(\nu_1) = \nu_1. \quad (\text{B3})$$

In the last equality we assume a bandwidth $E_{BW} \equiv N\delta \sim N^0$ to be finite.

Note that for a smooth function $g(\nu)$ the Legendre transform in Eq. (B1) gives the condition

$$g'(\nu_q) = q \quad (\text{B4})$$

while the prefactor in Eq. (B1) within a saddle-point approximation is given by

$$P(s \sim N^{-\nu}) ds = \sqrt{\frac{|g''(\nu_0)| \ln N}{2\pi}} N^{g(\nu)-1} d\nu, \quad (\text{B5})$$

where the smoothness of $g(\nu)$ at $\nu = \nu_0$ guarantees finiteness of the second derivative.

a. Correspondence between fractality of spectrum $f(b)$ and level spacing distribution $g(\nu)$. In order to understand how the levels ζ_n are distributed according to Eq. (3), one should take the extensive number of them $m \equiv N^{1-f(b)}$ and calculate the distance between

$$\zeta_{n+m} - \zeta_n \equiv \sum_{k=1}^m s_{n+k} \sim N^{-b}, \quad (\text{B6})$$

which gives an estimate of the number of levels in between. Please note that here, unlike Eq. (3), our control parameter will be the scaling of m , but not N^{-b} .

In order to find the correspondence between $f(b)$ and $g(\nu)$ we will use the method, developed in [37] to find a distribution of the extensive sums of multifractal i.i.d. random numbers. Indeed, for any $f(b)$ (or m) there can be two types of main contributions to Eq. (B6): the individual one and the collective one. In order to understand it, we will separate the sum of m elements into the “bins”, close to a certain ν , $s \in [N^{-\nu-d\nu}, N^{-\nu})$. For each of these bins, the number of elements in the corresponding part of the sum is given by

$$M_{\nu} \sim m \cdot P(s) ds \sim N^{g(\nu)-f(b)} d\nu. \quad (\text{B7})$$

Within the saddle-point approximation, the parameter b is determined by the maximum of the collective and individual contributions.

The individual contribution is given by a maximal $s_k \sim N^{-\nu^*}$ which appears in the above sum Eq. (B6) at least once, $M_{\nu^*} \sim N^0$. Thus, ν^* is given by the smaller solution of the equation

$$g(\nu^*) = f(b), \nu^* = b. \quad (\text{B8})$$

Thus, the amplitude of the sum is at least given by $N^{-b} \gtrsim N^{-\nu^*}$. The saturation of the latter inequality, $b \leq \nu^*$, gives $f(b) = g(b)$.

The collective contribution means that the corresponding number M_{ν} of elements $s_k \sim N^{-\nu}$, Eq. (B7), is extensive there, i.e., $g(\nu) > f(b)$. Similarly to Eq. (A5) changing the summation from k to ν in Eq. (B6) we obtain

$$N^{-b} \sim m \langle s \rangle_{M_{\nu} \gg 1} \sim \int_{g(\nu) > f(b)} d\nu N^{g(\nu)-f(b)-\nu}. \quad (\text{B9})$$

The latter integral for $g(\nu_1) > f(b)$ is given by $\nu = \nu_1$, i.e. by the mean-level spacing Eq. (B3). This gives $b = f(b)$ as $N\delta \sim N^{g(\nu_1)-\nu_1} \sim N^0$. Otherwise, $g(\nu_1) < f(b)$, the integral sits at $g(\nu^*) = f(b)$ and is dominated by the individual contribution.

Summarizing both cases, one obtains

$$N^{-b} \sim \begin{cases} N^{-\nu^*}, & g(\nu^*) = f(b), \quad g(\nu_1) < f(b) \\ N^{g(\nu_1)-f(b)-\nu_1}, & g(\nu_1) > f(b) \end{cases} \quad (\text{B10})$$

This result is quite straightforward as we know from the properties of $f(b)$ that its derivative cannot be larger than 1. The latter case corresponds to $d = 1$ in the fractal regime Eq. (4).

Hence, correspondence between $f(b)$ and $g(\nu)$ can be found to be

$$f(b) = \begin{cases} b, & b < \nu_1 \\ g(b), & b > \nu_1 \end{cases} \quad (\text{B11})$$

b. Log normal distribution as an example Let's consider a log-normal distribution of s , then $P(\nu)$ should be Gaussian, i.e., $g(\nu)$ is a parabola

$$g(\nu) = 1 - A(\nu - \nu_0)^2, \quad (\text{B12})$$

where we have parameterized it with the location of the maximum (typical $s_{typ} \sim N^{-\nu_0}$) and used the normalization condition $g(\nu_0) = 1$ from Eq. (B1). For this choice the prefactor in Eq. (16) is exact.

Taking into account also Eqs. (B3) and (B4), one obtains

$$\begin{aligned} 1 = g'(\nu_1) &= -2A(\nu_1 - \nu_0) \quad \Leftrightarrow \quad A = \frac{1}{2(\nu_0 - \nu_1)} > 0, \\ \nu_1 = g(\nu_1) &= 1 + \frac{\nu_1 - \nu_0}{2} \quad \Leftrightarrow \quad \nu_1 = 2 - \nu_0 < 1, \\ g(\nu) &= 1 - \frac{(\nu - \nu_0)^2}{4(\nu_0 - 1)}. \end{aligned} \quad (\text{B13})$$

Next, using Eqs. (7) and (8), for the log-normal distribution in Eq. (B13) one obtains the following equations for b

$$b = \gamma - 1, \quad (\text{B14})$$

at $\gamma < 3 - \nu_0$ and

$$b^2 + 2b(3\nu_0 - 4) + \nu_0^2 - 4(\nu_0 - 1)\gamma = 0 \quad (\text{B15})$$

at $\gamma > 3 - \nu_0$, with the solution

$$b = \begin{cases} \gamma - 1, & \gamma < 3 - \nu_0 \\ 4 - 3\nu_0 + 2\sqrt{(\nu_0 - 1)(\gamma + 2\nu_0 - 4)}, & \gamma > 3 - \nu_0 \end{cases} \quad (\text{B16})$$

leading to Eq. (17) in the main text.

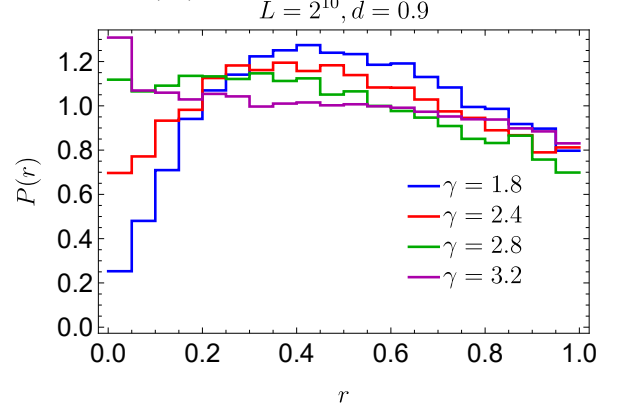


FIG. 7. Histogram of Probability density function of consecutive level spacing ratio r for diagonal disorder having Hausdorff dimension $d = 0.9$ for different $\gamma = 1.8, 2.4, 2.8, 3.2$ chosen near the “kink” in Fig. 5(d)

Appendix C: More details about r statistics

In Fig. 7 we show the histogram of probability density function of r defined in Eq. (18) for different γ to shed some light on the source of the second kink. From Fig. 5, we see that the second kink occurs inside the localized phase (for $d = 0.9$ at $\gamma > \gamma_{AT} \sim 2.2$). Looking at Fig. 7 we can verify that indeed already at $\gamma = 2.4$, the level repulsion is sufficiently weak. However the distribution undergoes further changes as we increase γ not only in the regime of $r \sim 0$, where we have increasing weight, but also in the region $r \sim 1$ due our choice of diagonal disorder. Deep inside the localized phase the energy levels are completely non-hybridized and the eigenenergies would be given by unperturbed diagonal elements. Since $P(r) \sim 1/r^{1-d}$, for $d \sim 1$ this indicates large weight at $r \sim 1$ which is seen for the $\gamma = 3.2$ line in the plot, which has a larger weight in that regime than $\gamma \sim 2.4, 2.8$. Hence the mean, $\langle r \rangle$ shows a rise at large values of γ for $d \sim 1$.